Electronic Supplementary Information (ESI)

Direct tuning of the band gap *via* electronically-active organic cations and large piezoelectric response in one-dimensional hybrid halides from first-principles

Gang Tang and Jiawang Hong *

School of Aerospace Engineering, Beijing Institute of Technology, Beijing, 100081, China.

E-mail: hongjw@bit.edu.cn

Computational Details

Density-functional theory (DFT) calculations were performed by using the projector-augmented wave (PAW) method, as implemented in the Vienna Ab initio Simulation Package (VASP) code.[1, 2] For structural properties, the generalized gradient approximation (GGA) formulated by Perdew, Burke, and Ernzerhof (PBE) was chosen as the exchange-correlation functional.[3] The plane-wave cut-off energy was set to 500 eV. The Γ-centered *k*-point meshes with *k*-spacing of ~0.2 $Å^{-1}$ were employed for sampling the Brillouin zone.[4] The lattice parameters and atomic positions were fully relaxed until the force on each atom is smaller than 0.01 eV/Å. Band structures and density of states were calculated by taking the spin-orbit coupling (SOC) interaction into account.[5] Based on the equation $m^* = \hbar^2/(\partial^2\varepsilon(k)/\partial k^2)$,[6] where $\varepsilon(k)$ are the band edge eigenvalues and k is the wavevector, the electron and hole effective masses were calculated using the finite difference method.[7, 8] The initial configurations of Sn^{2+}-doped $GAPbI_3$ and $C_7H_7^+$-doped $GAPbI_3$ with $1\times1\times3$ supercell were adopted for *ab initio* molecular dynamics (AIMD) simulations. Each 5 ps (time step is 1.0 fs) AIMD simulation was performed in the constant-volume and constant-temperature (300 K) (NVT) ensemble. The optical absorption spectra of $GAPbI_3$ and $C_7H_7^+$-doped $GAPbI_3$ are described by the complex dielectric function, *i.e.*, $\varepsilon(\omega) = \varepsilon_1(\omega) + i\varepsilon_2(\omega)$. Based on the dielectric function of investigated systems, the absorption coefficient $\alpha(\omega)$ can be given by the following equation: [9]

$$\alpha(\omega) = \frac{\sqrt{2}\omega\sqrt{\sqrt{\varepsilon_1(\omega)^2 + \varepsilon_2(\omega)^2} - \varepsilon_1(\omega)}}{c} \quad (1)$$

where ε_1 and ε_2 are the real and imaginary part of the dielectric function, respectively.

Structural Information

For $GAPbI_3$ with different octahedral connectivity, the 1D edge-sharing structure (see Figure S4a) is from the experimental data in Ref. 10; the 3D hypothetical corner-sharing structure is constructed by replacing all the $HC(NH_2)_2^+$ with $C(NH_2)_3^+$ in the $FAPbI_3$ (FA = $HC(NH_2)_2$), and the staring structure of $FAPbI_3$ is from Ref. 11; the 1D hypothetical face-sharing structure (see Figure S4c) is constructed by replacing all the Ge with Pb in the $GAGeI_3$, and the staring structure of $GAGeI_3$ is from Ref. 12. Prior to performing other calculations, we first examined the effect of different van der Waals

(vdW) corrections on the lattice constants for the edge-sharing structure. From Table S4, it can be seen that the combination of PBE functional and Grimme's D3 dispersion correction yields the most reasonable lattice constants in comparison to the experimental results. Therefore, we employed the PBE+D3 method for all calculations except the face-sharing structure. It is worth noting that for the face-sharing $GAPbI_3$, only the PBE+vdW-DF2 method well predicted reasonable lattice constants, and we chose it for all calculations of this structure.

For Sn^{2+}- or $C_7H_7^+$-doped $GAPbI_3$, different configurations were considered, and we chose the lowest total energy configuration for the final electronic properties calculations. The optimized structural parameters were summarized in Table S5.

Stability of $C_7H_7^+$-doped $GAPbI_3$ and Sn^{2+}-doped $GAPbI_3$

The thermodynamic stability of two doping systems against chemical decomposition was examined. For $C_7H_7^+$-doped $GAPbI_3$ and Sn^{2+}-doped $GAPbI_3$, the decomposition routes considered are:

$$[C(NH_2)_3]_{0.75}[C_7H_7]_{0.25}PbI_3 \rightarrow 3/4\ C(NH_2)_3I + 1/4\ C_7H_7I + PbI_2 \quad (2)$$

$$C(NH_2)_3Pb_{0.75}Sn_{0.25}I_3 \rightarrow C(NH_2)_3I + 3/4\ PbI_2 + 1/4\ SnI_2 \quad (3)$$

The calculated decomposition enthalpies ($\triangle H_d$) are 1.33 and 1.28 eV per formula unit (f.u.), respectively. It can be noted that both $C_7H_7^+$-doped $GAPbI_3$ and Sn^{2+}-doped $GAPbI_3$ show positive $\triangle H_d$ values, indicating that they are stable with respect to phase separation.

The mechanical stability of $C_7H_7^+$-doped $GAPbI_3$ and Sn^{2+}-doped $GAPbI_3$ was also examined. The calculated elastic stiffness constants (C_{ij}) are shown in Table S6. According to the mechanical stability criteria[13], two doping systems were checked through the following equations, and both $C_7H_7^+$-doped $GAPbI_3$ and Sn^{2+}-doped $GAPbI_3$ satisfy the fundamental mechanical stability criteria.

$$C_{11} > 0,\ C_{22} > 0,\ C_{33} > 0,\ C_{44} > 0,\ C_{55} > 0,\ C_{66} > 0, \quad (4)$$

$$[C_{11} + C_{22} + C_{33} + 2(C_{12} + C_{13} + C_{23})] > 0, \quad (5)$$

$$(C_{11} + C_{22} - 2\,C_{12}) > 0,\ (C_{11} + C_{33} - 2\,C_{13}) > 0,\ (C_{22} + C_{33} - 2\,C_{23}) > 0, \quad (6)$$

$$C_{11}C_{22} > C_{12}^2, \quad (7)$$

$$(C_{11}C_{22}C_{33} + 2C_{12}C_{13}C_{23} - C_{11}C_{23}^2 - C_{22}C_{13}^2 - C_{33}C_{12}^2) > 0. \quad (8)$$

Finally, the thermal stability of $C_7H_7^+$-doped $GAPbI_3$ and Sn^{2+}-doped $GAPbI_3$ was examined by performing *ab initio* molecular dynamics (AIMD) simulations at 300 K. As shown in Figure S5, the structure integrity of two doping systems is maintained after 5 ps AIMD simulation, indicating the thermal stability of $C_7H_7^+$-doped $GAPbI_3$ and Sn-doped $GAPbI_3$ at the room temperature.

Calculation of Elastic Stiffness and Piezoelectric Tensors

For $GAPbI_3$ with the $Pna2_1$ space group, the elastic stiffness tensors are calculated in the form of the stiffness tensors (C), presented as a 6×6 matrix:[14]

$$\begin{pmatrix} \boldsymbol{C_{11}} & \boldsymbol{C_{12}} & \boldsymbol{C_{13}} & \mathbf{0} & \mathbf{0} & \mathbf{0} \\ \boldsymbol{C_{12}} & \boldsymbol{C_{22}} & \boldsymbol{C_{23}} & \mathbf{0} & \mathbf{0} & \mathbf{0} \\ \boldsymbol{C_{13}} & \boldsymbol{C_{23}} & \boldsymbol{C_{33}} & \mathbf{0} & \mathbf{0} & \mathbf{0} \\ \mathbf{0} & \mathbf{0} & \mathbf{0} & \boldsymbol{C_{44}} & \mathbf{0} & \mathbf{0} \\ \mathbf{0} & \mathbf{0} & \mathbf{0} & \mathbf{0} & \boldsymbol{C_{55}} & \mathbf{0} \\ \mathbf{0} & \mathbf{0} & \mathbf{0} & \mathbf{0} & \mathbf{0} & \boldsymbol{C_{66}} \end{pmatrix}$$

The piezoelectric stress tensors (e) are calculated in the following form, presented as a 3×6 matrix:[14]

$$\begin{pmatrix} \mathbf{0} & \mathbf{0} & \mathbf{0} & \mathbf{0} & \boldsymbol{e_{15}} & \mathbf{0} \\ \mathbf{0} & \mathbf{0} & \mathbf{0} & \boldsymbol{e_{24}} & \mathbf{0} & \mathbf{0} \\ \boldsymbol{e_{31}} & \boldsymbol{e_{32}} & \boldsymbol{e_{33}} & \mathbf{0} & \mathbf{0} & \mathbf{0} \end{pmatrix}$$

The finite differences method and density functional perturbation theory (DFPT) method were employed to calculate the elastic stiffness tensors and piezoelectric stress tensors, respectively.[15, 16] For both calculations, the 3×2×7 gamma centred k-point grid and 700 eV cut-off energy were chosen.

Based on the obtained C_{ij} and e_{ij} tensors, using the following equations,[16, 17] the d_{ij} coefficients reported in the main text can be obtained.

$$d_{ij} = \sum_{k=1}^{6} e_{ik} S_{kj}, \quad S_{ij} = (C_{ij})^{-1} \tag{9}$$

$$d_{15} = e_{15} \times S_{55}, \quad d_{24} = e_{24} \times S_{44} \tag{10}$$

$$d_{31} = e_{31} \times S_{11} + e_{32} \times S_{21} + e_{33} \times S_{31} \tag{11}$$

$$d_{32} = e_{31} \times S_{12} + e_{32} \times S_{22} + e_{33} \times S_{32} \tag{12}$$

$$d_{33} = e_{31} \times S_{13} + e_{32} \times S_{23} + e_{33} \times S_{33} \tag{13}$$

Where S_{ij} is the compliance matrix.

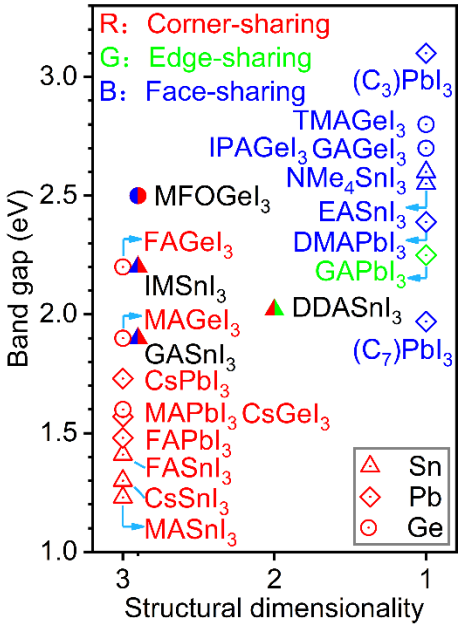

Figure S1. Experimental optical band gaps of 1D, 2D, and 3D ABI_3 (A = organic molecule or Cs; B = Pb, Sn, and Ge) iodide compounds. The red, green and blue symbols indicate the corner-, edge-, and face-sharing connectivity of $[BI_6]$ octahedra in ABI_3, respectively. The structural dimensionalities of $MFOGeI_3$, $IMSnI_3$, and $GASnI_3$ are all quasi-3D and are labelled as mixture colour. The abbreviation of organic molecule A in the figure is: "C_3": $(CH_3)_3S$; "C_7": C_7H_7; "DDA": $CH_3(CH_2)_{11}NH_3$; "DMA": $(CH_3)_2NH_2$; "TMA": $(CH_3)_3NH$; "NMe_4": $(CH_3)_4N$; "IM": $C_3N_2H_5$; "IPA": $(CH_3)_2C(H)NH_3$; "MFO": $CH_3C(NH_2)_2$; "EA": $CH_3CH_2NH_3$; "GA": $C(NH_2)_3$; "FA": $HC(NH_2)_2$; "MA": CH_3NH_3. The detailed data are given in Table S7.

Table S1. Bond lengths and bond angles from experimental and calculated $GAPbI_3$ with different structures.

	Pb−I bond length (AVG) (Å)	**Pb−I−Pb bond angle (deg)**
Edge-sharing (Expt.[10])	3.07-3.56 (3.28)	91-92
Edge-sharing	3.15-3.36 (3.25)	92
Face-sharing	3.30-3.42 (3.36)	74
Corner-sharing	3.23-3.24 (3.23)	169-170

Table S2. The average electron (m_e) and hole (m_h) effective masses along the high symmetry directions near the band gap edges for $GAPbI_3$ with different structures estimated from the PBE+SOC calculated band structures. m_0 is the electron static mass.

[PbI_6] Connectivity	**m_e/m_0**			**m_h/m_0**		
	F-Q	Q-Z	AVG	F-Q	Q-Z	AVG
Corner-sharing	0.17	0.17	0.17	0.37	0.35	0.36
	Γ-X	X-U	AVG	Z-Γ	Γ-X	AVG
Edge-sharing	1.49	0.82	1.15	0.81	1.08	0.94
	D-Z	Z-Γ	AVG	C-Y	Y-Γ	AVG
Face-sharing	5.01	2.97	3.99	10.81	2.48	6.64

Table S3. Calculated piezoelectric stress constants (e_{ij}), elastic constants (C_{ij}), and piezoelectric strain constants (d_{ij}) for zinc oxide (ZnO). Other theoretical and experimental results are also shown for comparison.

	e_{ij} (C/m^2)			**C_{ij} (C/m^2)**						**d_{ij} (pC/N)**		
	e_{31}	**e_{33}**	**e_{15}**	**C_{11}**	**C_{33}**	**C_{44}**	**C_{66}**	**C_{12}**	**C_{13}**	**d_{31}**	**d_{33}**	**d_{15}**
This work	-0.63	1.22	-0.46	202	219	36	39	125	110	-5.7	11.3	-12.8
Calc.[16]	-0.67	1.28	-0.53	-	-	-	-	-	-	-5.5	10.9	-13.1
Calc.[18]	-0.55	1.19	-0.46	246	246	56	-	127	105	-3.7	8.0	-8.2
Expt.[19]	-0.62	0.96	-0.37	209	216	44	-	120	104	-5.1	12.3	-8.3
Expt.[20]	-0.61	1.15	-	-	-	-	-	-	-	-	-	-

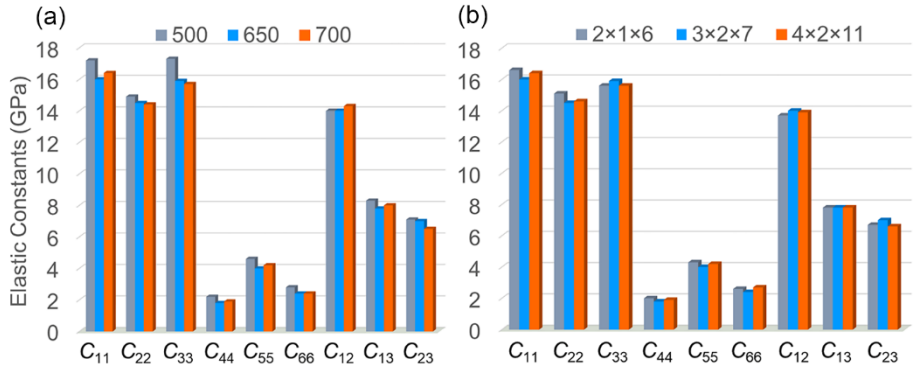

Figure S2. Graphs showing the convergence in predicted elastic constants for $GAPbI_3$ using different cut-off energy and *k*-point mesh. Note that for the convergence tests of cut-off energy, the *k*-point mesh is 3×2×7. And for the convergence tests of *k*-point mesh, the cut-off energy is 650 eV.

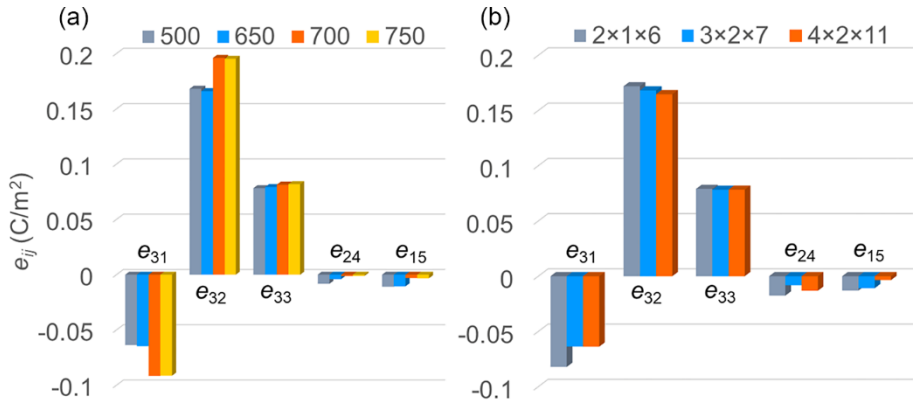

Figure S3. Graphs showing the convergence in predicted piezoelectric stress constants for $GAPbI_3$ using different cut-off energy and *k*-point mesh. Note that for the convergence tests of cut-off energy, the *k*-point mesh is 3×2×7. And for the convergence tests of *k*-point mesh, the cut-off energy is 650 eV.

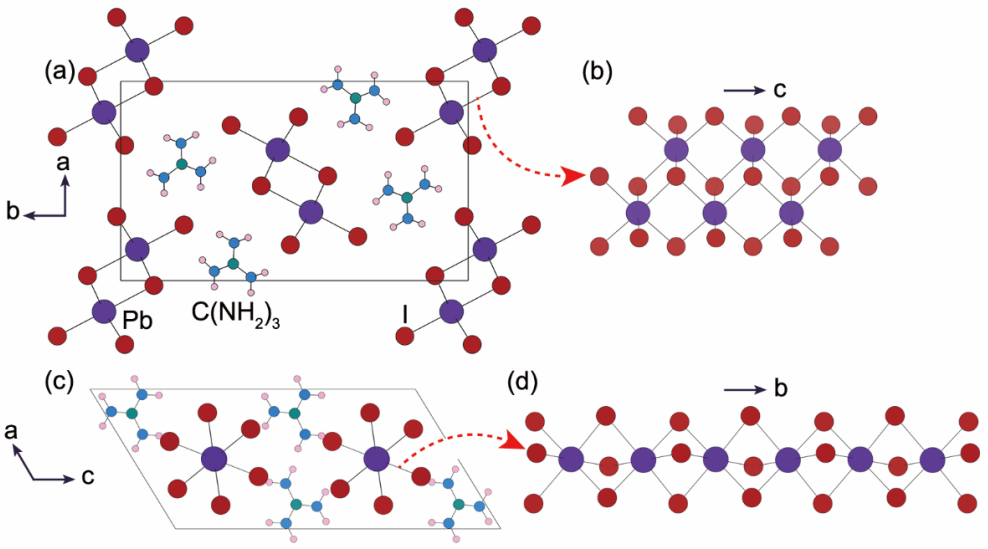

Figure S4. Crystal structures of (a) edge-sharing and (c) face-sharing $GAPbI_3$. Note that (b) displays the edge-sharing connectivity of [PbI_6] octahedra along the *c* direction for (a), and (d) displays the face-sharing connectivity of [PbI_6] octahedra along the *b* direction for (c).

Table S4. Experimental and calculated lattice parameters with different van der Waals (vdW) corrections for the edge-sharing $GAPbI_3$. Note that percentage differences of calculated parameters from the experimental ones are shown in brackets.

Methods	***a* (Å)**	***b* (Å)**	***c* (Å)**
Expt.[10]	11.990	20.880	4.476
DFT-D3	11.904 (-0.72%)	20.737 (-0.68%)	4.500 (-0.54%)
PBEsol	10.453 (+12.82%)	24.180 (+15.80%)	4.567 (+2.03%)
vdW-DF2	12.152 (+1.35%)	21.087 (+0.99%)	4.667 (+4.27%)
optB86b-vdW	11.920 (-0.58%)	20.635 (-1.17%)	4.427 (-1.09%)

Table S5. Calculated structural parameters for Sn^{2+}-doped and $C_7H_7^+$-doped $GAPbI_3$.

	Sn^{2+}-doped	**$C_7H_7^+$-doped**
a (Å)	11.869	11.683
b (Å)	20.735	21.813
c (Å)	4.486	4.561
α (deg)	89.86	89.35
β (deg)	89.97	92.02
γ (deg)	90.02	93.22
V (Å^3)	1104.01	1159.64
Pb−I bond length (Å)	3.15-3.36	3.12-3.39

Pb−I−Pb bond angle (deg)	82-88	88-91
Sn−I bond length (Å)	3.09-3.33	-
Pb−I−Sn bond angle (deg)	92	-

Table S6. Elastic stiffness constants C_{ij} of $C_7H_7^+$-doped and Sn^{2+}-doped $GAPbI_3$.

	C_{ij} (GPa)								
	C_{11}	C_{12}	C_{13}	C_{23}	C_{22}	C_{33}	C_{44}	C_{55}	C_{66}
$C_7H_7^+$-doped	10.6	12.1	8.1	8.2	18.5	14.9	2.9	2.1	3.0
Sn^{2+}-doped	16.6	14.1	7.9	7.2	17.2	15.9	2.8	2	4.5

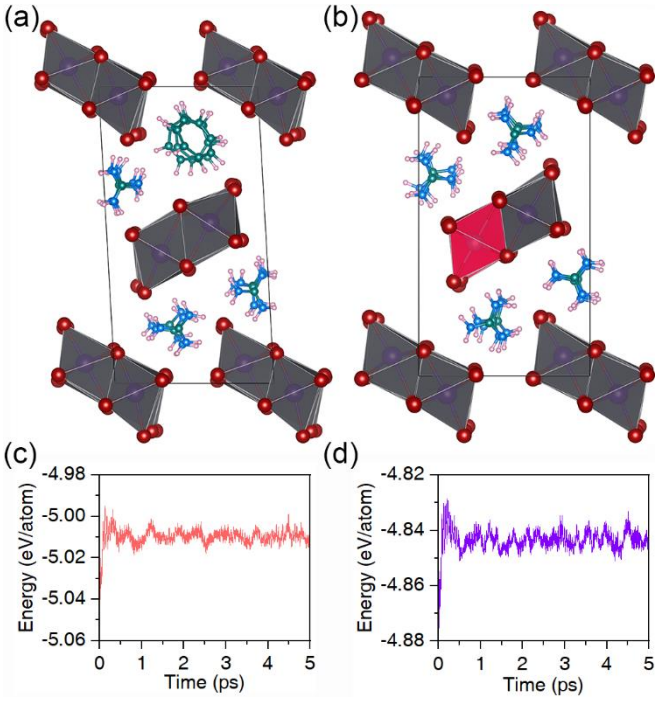

Figure S5. The snapshots of structure (after 5 ps) and the free energy fluctuations of (a and c) $C_7H_7^+$-doped and (b and d) Sn^{2+}-doped $GAPbI_3$, with *ab initio* molecular dynamic (AIMD) simulations at 300 K.

Table S7. Experimental structural data (*i.e.*, space group and structural dimensionality), octahedral connectivity, and band gaps (E_g) of some iodide compounds ABI_3 (A = organic molecules or Cs; B = Pb, Sn, and Ge).

Materials	Space group	Octahedral connectivity	Structural dimensionality	E_g (eV)	Ref.
$CsPbI_3$	*Pm-3m*	Corner-sharing	3	1.73	21
$CsSnI_3$	*Pnma*	Corner-sharing	3	1.3	22
$CsGeI_3$	*R3m*	Corner-sharing	3	1.6	12
$MAPbI_3$	*I4cm*	Corner-sharing	3	1.57	23

$MASnI_3$	*P*4*mm*	Corner-sharing	3	1.23	24
$MAGeI_3$	*R*3*m*	Corner-sharing	3	1.9	12
$FAPbI_3$	*Pm*-3*m*	Corner-sharing	3	1.48	25
$FASnI_3$	*Amm*2	Corner-sharing	3	1.41	24
$FAGeI_3$	*R*3*m*	Corner-sharing	3	2.2	12
$GAPbI_3$	$Pna2_1$	Edge-sharing	1	2.25	10
$GAGeI_3$	$P2_1/c$	Face-sharing	1	2.7	12
$GASnI_3$	$P6_3/m$	Corner/Face-sharing	quasi 3	1.9	24
$MFOGeI_3$	$P2_1$	Corner/Face-sharing	quasi 3	2.5	12
$TMAGeI_3$	$P6_3$	Face-sharing	1	2.8	12
$IPAGeI_3$	*I*-42*d*	Face-sharing	1	2.7	12
$TMASnI_3$	*R*3*c*	Face-sharing	1	2.55	24
$IMSnI_3$	*Pc*	Corner/Face-sharing	quasi 3	2.2	24
NMe_4SnI_3	$P6_3/m$	Face-sharing	1	2.6	24
$(C_3)PbI_3$	$P6_3mc$	Face-sharing	1	3.1	26
$DDASnI_3$	*P*-1	Corner/Edge-sharing	2	2.02	27
$DMAPbI_3$	$P6_3/mmc$	Face-sharing	1	2.39	28
$(C_7)PbI_3$	*Pnma*	Face-sharing	1	1.97	29

The abbreviation of organic molecule A in the Table is: "C_3": $(CH_3)_3S$; "C_7": C_7H_7; "DDA": $CH_3(CH_2)_{11}NH_3$; "DMA": $(CH_3)_2NH_2$; "TMA": $(CH_3)_3NH$; "NMe_4": $(CH_3)_4N$; "IM": $C_3N_2H_5$; "IPA": $(CH_3)_2C(H)NH_3$; "MFO": $CH_3C(NH_2)_2$; "EA": $CH_3CH_2NH_3$; "GA": $C(NH_2)_3$; "FA": $HC(NH_2)_2$; "MA": CH_3NH_3.

References:

1 G. Kresse and J. Furthmüller, *Comput. Mater. Sci.*, 1996, **6**, 15-50.

2 G. Kresse and D. Joubert, *Phys. Rev. B: Condens. Matter Mater. Phys.*, 1999, **59**, 1758.

3 J. P. Perdew, K. Burke and M. Ernzerhof, *Phys. Rev. Lett.*, 1996, **77**, 3865.

4 P. E. Blöchl, O. Jepsen and O. K. Andersen, *Phys. Rev. B: Condens. Matter Mater. Phys.*, 1994, **49**, 16223.

5 A. V. Krukau, O. A. Vydrov, A. F. Izmaylov and G. E. Scuseria, *J. Chem. Phys.*, 2006, **125**, 224106.

6 G. Giorgi, J.-I. Fujisawa, H. Segawa, and K. Yamashita, *J. Phys. Chem. Lett.*, 2013, **4**, 4213-4216.

7 G. Volonakis, M. R. Filip, A. A. Haghighirad, N. Sakai, B. Wenger, H. J. Snaith, and F. Giustino, *J. Phys. Chem. Lett.*, 2016, **7**, 1254–1259.

8 T. Low, A. S. Rodin, A. Carvalho, Y. Jiang, H. Wang, F. Xia, and A. H. C. Neto, *Phys. Rev. B: Condens. Matter Mater. Phys.*, 2014, **90**, 075434.

9 U. G. Jong, C. J. Yu, J. S. Ri, N. H. Kim and G. C. Ri, *Phys. Rev. B: Condens. Matter Mater. Phys.*, 2016, **94**, 125139.

10 A. D. Jodlowski, A. Yépez, R. Luque, L. Camacho and G. de Miguel, *Angew. Chem., Int. Ed.*, 2016, **55**, 14972-14977.

11 M. Bokdam, T. Sander, A. Stroppa, S. Picozzi, D. D. Sarma, C. Franchini and G. Kresse, *Sci. Rep.*, 2016, **6**, 28618.

12 C. C. Stoumpos, L. Frazer, D. J. Clark, Y. S. Kim, S. H. Rhim, A. J. Freeman, J. B. Ketterson, J. I. Jang and M. G. Kanatzidis, *J. Am. Chem. Soc.*, 2015, **137**, 6804-6819.

13 F. Mouhat and F.-X. Coudert, *Phys. Rev. B: Condens. Matter Mater. Phys.*, 2014, **90**, 224104.

14 J. F. Nye, Physical Properties of Crystals: Their Representation by Tensors and Matrices, Oxford University Press, New York, U.S.A.; 1985.

15 Y. L. Page, *Phys. Rev. B: Condens. Matter Mater. Phys.*, 2002, **65**, 104104.

16 X. Wu, D. Vanderbilt and D. R. Hamann, *Phys. Rev. B: Condens. Matter Mater. Phys.*, 2005, **72**, 035105.

17 G. Gou and J. M. Rondinelli, *Adv. Mater. Interfaces*, 2014, **1**, 1400042.

18 M. Catti, Y. Noel and R. *J.* Dovesi, *Phys. Chem. Solids*, 2003, **64**, 2183-2190.

19 Landolt-Bo ¨rnstein, O. Madelung (Ed.), New Series, Group III: Solid State Physics, Low Frequency Properties of Dielectric Crystals: Piezoelectric, Pyroelectric and Related Constants, Springer Press: Berlin, German; 1993.

20 H.Y.S. Al-Zahrani, J. Pal and M.A. Migliorato, *Nano Energy*, 2013, **2**, 1214-1217.

21 G. E. Eperon, G. M. Paternò, R. J. Sutton, A. Zampetti, A. A. Haghighirad, F. Cacialli and H. J. Snaith, *J. Mater. Chem. A*, 2015, **3**, 19688-19695.

22 I. Chung, J. H. Song, J. Im, J. Androulakis, C. D. Malliakas, H. Li, A. J. Freeman, J. T. Kenney and M. G. Kanatzidis, *J. Am. Chem. Soc.*, 2012, **134**, 8579-8587.

23 C. C. Stoumpos, C. D. Malliakas and M. G. Kanatzidis, *Inorg. Chem.*, 2013, **52**, 9019-9038.

24 C. C. Stoumpos, L. Mao, C. D. Malliakas and M. G. Kanatzidis, *Inorg. Chem.*, 2017, **56**, 56-73.

25 G. E. Eperon, S. D. Stranks, C. Menelaou, M. B. Johnston, L. M. Herz and H. J. Snaith, *Energy Environ. Sci.*, 2014, **7**, 982-988.

26 A. Kaltzoglou, C. C. Stoumpos, A. G. Kontos, G. K. Manolis, K. Papadopoulos, K. G. Papadokostaki, V. Psycharis, C. C. Tang, Y. K. Jung, A. Walsh, M. G. Kanatzidis and P. Falaras, *Inorg. Chem.*, 2017, **56**, 6302-6309.

27 Z. Xu and D. B. Mitzi, *Inorg. Chem.*, 2003, **42**, 6589-6591.

28 A. Mancini, P. Quadrelli, G. Amoroso, C. Milanese, M. Boiocchi, A. Sironi, M. Patrini, G. Guizzetti and L. Malavasi, *J. Solid State Chem.*, 2016, **240**, 55-60.

29 A. E. Maughan, J. A. Kurzman and J. R. Neilson, *Inorg. Chem.*, 2015, **54**, 370-378.